# Exploring Sediment Compaction in Experimental Deltas: towards a meso-scale understanding of coastal subsidence patterns

**Samuel M. Zapp[1,2], Kelly Sanks[1,3], Jose Silvestre[3], John B. Shaw[1], Ripul Dutt[3], and Kyle M. Straub[3]**

[1]Department of Geosciences, University of Arkansas, Fayetteville, 72701, USA
[2]Department of Oceanography and Coastal Science, Louisiana State University, Baton Rouge, LA, USA
[3]Department of Earth and Environmental Sciences, Tulane University, New Orleans, LA, USA

**Key Points:**

- The addition of a proxy for marsh sedimentation increases subsidence due to sediment compaction in two laboratory delta experiments
- Subsidence is spatio-temporally variable and dominantly shallow in the experiment with a marsh proxy
- Subsidence rates, even across large areas, are highly variable on short timescales

Corresponding author: Samuel M. Zapp, szapp1@lsu.edu

## Abstract

We present the first investigation of subsidence due to sediment compaction and consolidation in two laboratory-scale river delta experiments. Spatial and temporal trends in subsidence rates in the experimental setting may elucidate behavior which cannot be directly observed at sufficiently long timescales, except for in reduced scale models such as the ones studied. We compare subsidence between a control experiment using steady boundary conditions, and an otherwise identical experiment which has been treated with a proxy for highly compressible marsh deposits. Both experiments have non-negligible compactional subsidence rates across the delta-top, comparable in magnitude to our boundary condition relative sea level rise of 250 μm/h. Subsidence in the control experiment (on average 54 μm/h) is concentrated in the lowest elevation (<10mm above sea level) areas near the coast and is likely due to creep induced by a rising water table near the shoreface. The treatment experiment exhibits larger (on average 126 μm/h) and more spatially variable subsidence rates controlled mostly by compaction of recent marsh deposits within one channel depth (∼10 mm) of the sediment surface. These rates compare favorably with field and modeling based subsidence measurements both in relative magnitude and location. We find that subsidence "hot spots" may be relatively ephemeral on longer timescales, but average subsidence across the entire delta can be variable even at our shortest measurement window. This suggests that subsidence rates in a given decade or century may exceed thresholds for marsh platform drowning, even if the long term trend does not.



## Plain Language Summary

Coastal and deltaic wetlands sit very near sea level. They accumulate a compressible mixture of organic material and mud which is deposited by tides and/or overbank flooding from rivers. As a result, these wetland environments can rapidly build elevation to keep pace with a significant amount of relative sea level rise. Over time, more sediment is delivered on top of the initially porous surface layers and they become compacted as they are buried, contributing to a downward movement of the land surface known as subsidence. Subsidence is a hazard that threatens infrastructure and worsen coastal flooding. Here we examine the spatial and temporal patterns of subsidence in a small (about 2 $m^2$) physical delta experiment which includes a compressible proxy for wetland sediments. We find that subsidence is significantly higher where these wetland sediments have recently been deposited, and driven by their compaction in the very shallow subsurface.


## 1 Introduction

Subsidence, the downward directed movement of the Earth surface, exerts a fundamental physical control on river deltas. Summed with changes in eustatic sea level, subsidence increases relative sea level rise (RSLR) which controls the equilibrium size of a delta, and the dynamics of its channels and marshes (Liang et al., 2016; Moodie & Passalacqua, 2021; R. Morton et al., 2006). Sediment deficits and projections of future sustainability of deltas often include subsidence as one of the largest uncertainties (K. M. Sanks et al., 2020; Shirzaei et al., 2021). Hence, subsidence affects the dynamic ecosystems and several hundred million people that live on river deltas.

The stability of coastal wetlands is closely coupled to subsidence because they exist within the intertidal zone and accrete as a function of elevation relative to sea level (Morris et al., 2002; Cahoon et al., 2019). These threatened environments provide valuable ecosystem services including storm surge protection, carbon sequestration, and water quality regulation (Engle, 2011). Wetland retreat is expected to respond non-linearly with future RSLR projections (Mariotti, 2020; Tornqvist et al., 2020). In South Louisiana alone, over 5,000 $km^2$ of coastal wetlands have been lost since 1930 (Couvillion et al.,

2017), largely due to high, spatio-temporally variable subsidence rates from the compaction of highly compressible marsh deposits in the shallow subsurface (Törnqvist et al., 2008). On modern river deltas, subsidence within the top several meters of stratum, often including a significant amount of organic material, can dominate background RSLR (eustatic sea level rise plus tectonic regional subsidence) over large areas by as much as an order of magnitude, at least on short timescales (Jankowski et al., 2017; Erban et al., 2014; Zumberge et al., 2022).

Measured subsidence rates on river deltas worldwide are both highly spatially and temporally variable. While subsidence rates over annual to decadal timescales can approach a centimeter per year on the Mississippi River Delta (Nienhuis et al., 2017), there is disagreement about the upper bound of annual subsidence rates and whether or not subsidence maxima correlate with geologic controls such as Holocene deposit thickness (Jankowski et al., 2017; Byrnes et al., 2019). Millennial scale subsidence rates are consistently estimated to be significantly lower (Kooi & de Vries, 1998; Meckel et al., 2006; van Asselen, 2011; Frederick et al., 2019). It remains unclear if areas of high subsidence can persist on century and longer timescales due to a lack of direct measurement going back further than about 15 years. Additionally, the overprinting of several possible subsidence mechanisms including sediment compaction, faulting, anthropogenic soil drainage and deep fluid withdrawal make it difficult to understand which processes are driving the complexity of observed subsidence rates (Dokka, 2006; Yuill et al., 2009; Chang et al., 2014). Understanding the degree to which natural processes and human activity each impact different subsidence mechanisms is crucial to proposed land loss mitigation plans such as sediment diversions and wetland restoration, which are planned on decadal to centennial timescales (*Louisiana's Comprehensive Master Plan for a Sustainable Coast*, 2017).

Our understanding of the co-evolution between delta morphodynamics, marsh growth, and emergent subsidence remains relatively limited. This incomplete understanding can be attributed to our inability to observe the processes of delta evolution (i.e. aggradation, channel incision, avulsion) and marsh platform growth over sufficiently long "mesotimescales" ($10^2$-$10^5$ years), as well as difficulty isolating the various forcing conditions that drive morphodynamic change and mechanisms that contribute to coastal subsidence (Hoyal & Sheets, 2009; Yuill et al., 2009).

Here we describe the autogenic subsidence behavior of two laboratory scale delta experiments, one treated with a proxy for marsh deposits (TDWB-19-2, hereafter called the treatment experiment) and one untreated experiment (TDB-18-1, hereafter called the control experiment), in order to better understand how the coupling between deltas and marshes impacts the spatio-temporal variability of subsidence rates throughout delta evolution. Reduced-scale experiments are effective at creating analogous kinematics and spatial architecture to autogenic behavior observed in field deltas (Paola et al., 2009). They are a particularly useful tool to understand "meso-scale" delta evolution that cannot be fully captured by continuous field measurement during active morphodynamic changes, nor reconstructed by stratigraphic interpretation (Paola et al., 2009). Our setup is designed to dissociate background relative sea level rise applied as a boundary condition ($RSLR_b$; meant to represent both tectonic subsidence and eustatic sea level rise) from spatially and temporally variable subsidence that emerges within the experiment ($\sigma_s$).

This study is part of a larger project (including K. M. Sanks et al. (2022)) which aims to assess the impact of marshes on a wide range of deltaic processes, from delta-top kinematics to stratigraphic patterns. No studies have previously described autogenic subsidence due to sediment compaction (hereafter, just subsidence) in a delta experiment. We hypothesize that the addition of the marsh proxy in the treatment experiment will generate significant subsidence across the portion of the delta that regularly receives marsh deposits. In this case, subsidence rates will likely be correlated with underlying marsh

deposit thickness. If subsidence rates are sufficiently large over long enough timescales, they could influence a wide range of geomorphic processes.

## 2 Methods

### 2.1 Experimental Setup

We analyze two delta experiments conducted at the Tulane Sediment Dynamics and Stratigraphy Lab. The experiments have identical boundary conditions, and approached a dynamic equilibrium state under constant forcing conditions of sea level rise rate ($RSLR_b$), basin geometry (2.8 m across with an open seaward boundary), and water ($Q_w$) and sediment discharge ($Q_s$) listed in Table 1. Each experiment was allowed to prograde for 120 hours before hour zero of runtime. The treatment experiment differed only in that a proxy for marsh sedimentation was applied to regions near sea level, resulting in about 8% of the final deposit mass and 15% of the final deposit volume (K. M. Sanks et al., 2022). Therefore, significant statistical differences in subsidence rates can be attributed to the impact of the marsh proxy deposits.

**Table 1.** Boundary conditions of both experiments.

| **Delta Experiment** | **Experiment Run Time (h)** | $Q_w$ **($m^3/s$)** | $Q_s$ **(kg/h)** | $RSLR_b$ **(mm/h)** | **Sediment Mixture** |
|---|---|---|---|---|---|
| Control (TDB-18-1) | 560 | $1.72*10^4$ | 1.40 | 0.25 | Strongly cohesive mixture (Straub et al., 2015) |
| Marsh (TDWB-19-2) | 560 | $1.72*10^4$ | 1.40 | 0.25 | Strongly cohesive mixture (Straub et al., 2015)<br>EPK marsh proxy (200g/2hr) |

Topography was measured with a Lidar scanner to create digital elevation models (DEMs) with a 5 x 5 mm planform grid, and a sub-mm vertical resolution (Text S2). In the control experiment, scans were collected at the beginning of each run hour. In the treatment, scans were collected at the beginning of every even run hour directly before the marsh proxy was dispensed, as well as 48 minutes into each run hour after the marsh was dispensed. This allows for measurement of subsidence at the two-hour timescale, as well as the initial thickness of each marsh deposit.

The marsh proxy was distributed based on a simple conceptual model relating primary production in salt marshes to elevation relative to sea level (Morris et al., 2002). As such, the distribution patterns here are primarily intended to mimic marshes present in coastal settings. Every two hours, a DEM was averaged at the 0.015 $m^2$ scale on a hexagonal grid in order to identify suitable elevations for marsh deposition (Fig. 1a). The marsh proxy (Edgar Plastic Kaolin, or EPK) was distributed to each hexagon as a function of this averaged elevation (mm) relative to current sea level (rsl). All binned locations with an average elevation between -9 mm and 5 mm rsl (hereafter referred to as the "marsh window") received marsh sediment from a vibrating sieve (Fig. 1b). The proxy's porosity when settling through water was measured in pre-experiment trials to be roughly 90% when first deposited. This gives it significantly more compaction potential than the fluvially-introduced clastic sediment. The sediment mixture delivered by river transport to both experiments ranges in grain size from coarse sand to clay and contains a polymer to increase sediment cohesion. It has been described in K. M. Straub et al. (2015).

Cores taken from the control experiment have porosities of 50-60% averaged across the thickness of the entire stratigraphic package.

This setup was not meant to imitate any particular field setting, but designed to create a steady-state scenario where the unstable (-9 to -5 mm rsl) and stable (0 to 5 mm rsl) marshes would inevitably lose elevation in the absence of mineral sediment nourishment, while maximally productive marsh (-5 to 0 mm rsl; Fig. 1b) areas would outpace $RSLR_b$, at least over short timescales. All marshes could theoretically drown if $\sigma_s$ became sufficiently high. Initial marsh deposit thicknesses from -9 to -5 mm and 0 to 5 mm accreted at 0.45 times $RSLR_b$, and deposits in the -5 to 0 mm elevation range accreted 1.1 times $RSLR_b$. Total drowning of the marsh platform would occur under mineral sediment input equal to $RSLR_b$ (our long-term steady-state assumption) if $\sigma_s$ were to exceed $RSLR_b$ by a factor of 1.1 (or 275 $\mu$m) for enough time to submerge any preexisting elevation capital. On shorter timescales, where mineral sedimentation from the fluvial system could be entirely absent in some areas, $\sigma_s$ values in excess of 0.1 times $RSLR_b$ (or 25 $\mu$m) would cause all marshes to lose elevation.

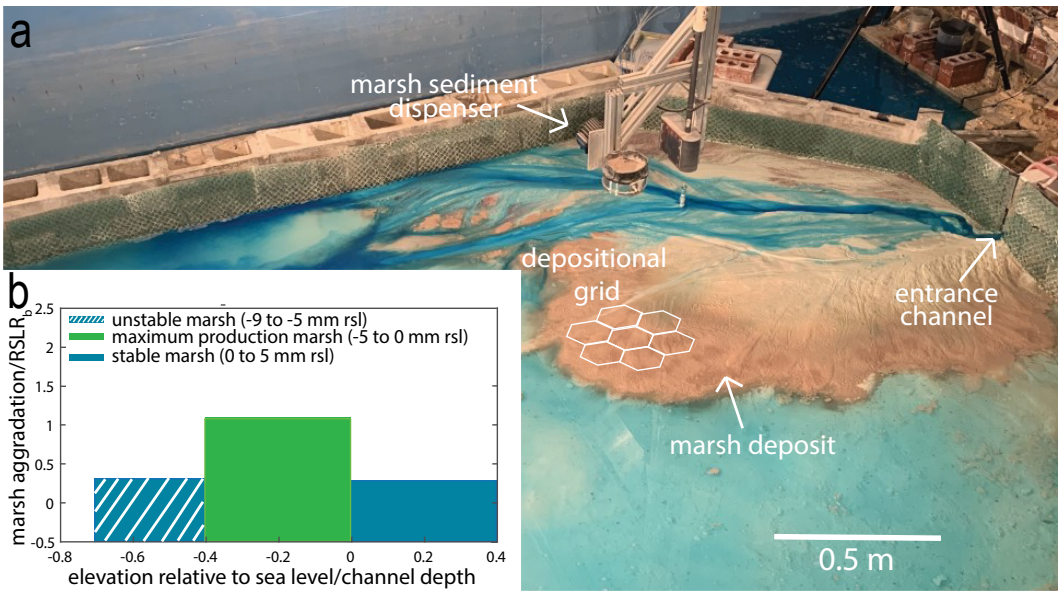


**Figure 1.** (a) An image of the treatment experiment during a marsh distribution cycle. The metal apparatus is a sieve mounted to a low-frequency vibrator which shakes out marsh proxy. The darker brown sediment is exposed marsh deposits. White hexagons represent the grid that marsh proxy was distributed over. (b) Elevation based rules for marsh deposition rates. Average channel depth of treatment experiment is $\approx$ 14 mm. The maximum production marsh region (-5 to 0 mm rsl) aggrades faster than $RSLR_b$, while unstable (well below sea level) and stable (above sea level) regions aggrade slower than $RSLR_b$. Modified from K. M. Sanks et al. (2022).

The cohesive "clastic" sediment mixture delivered by river transport to both experiments ranges in grain size from coarse sand to clay and contains a polymer to increase sediment cohesion (K. M. Straub et al., 2015; Li et al., 2017). Cores taken from the control experiment have porosities of 50-60% averaged across the thickness of the entire stratigraphic package.

### 2.2 Subsidence and Marsh Thickness Maps

Subsidence maps for both experiments were generated by differencing DEMs and screening out areas that were flooded by sea level or that received surface water flow at some point during the timestep. This was done to remove all sediment transport processes and isolate subsidence in "quiescent" areas. Areas covered by surface water were removed by a color threshold screen. Differenced DEM values lower than -1000 $\mu$m or greater than 5000 $\mu$m were considered erroneous and removed from the dataset.

Control experiment DEMs were differenced by appropriately screening each scan, subtracting the previous dry scan from a given scan, and then summing the resulting two-hour DEMs of difference. The treatment experiment DEMs were differenced by subtracting the wet scan collected 72 minutes prior from each dry scan. This was done to exclude marsh accretion in the first 48 minutes of each two-hour period of run time. The resulting subsidence maps were then multiplied by a correction factor of 120/72 to account for "lost" time and make them equivalent to two-hour DEMs of difference. Therefore, subsidence rates can be compared between the experiments at a two-hour temporal resolution. Subsidence rates were also compared at ten-hour time steps by summing consecutive two-hour subsidence maps. Subsidence rates were also compared at ten-hour time steps by summing consecutive two-hour subsidence maps and excluding points which did not return a value each time step.

An initial thickness map of each marsh deposit was separately quantified by differencing the wet scan taken right after distribution and the dry scan taken right before, then screening out areas outside of the marsh window. Areas receiving surface water were excluded in the same manner as in the subsidence maps.

Marsh maps derived from Lidar scans were stacked to create a "synthetic stratigraphy" representing the total uncompacted thickness of the marsh maps at each location. The marsh maps do not account for submarine marsh deposition, so they do not equate to total initial marsh deposit thickness, only subaerial marsh thickness. However, this marsh thickness can be normalized by the thickness of the final deposit to yield a synthetic marsh fraction which is comparable to the directly measured marsh thickness from stratigraphy.

### 2.3 Measurements of Marsh Deposits in Stratigraphy

At the end of the treatment experiment, the deposit was sectioned along strike parallel to the entrance channel at 10 cm intervals. The thicknesses of buried marsh deposits were measured at a number of locations. Several measurements of porosity (used to calculate void ratio) were taken from individual seams of preserved marsh proxy at various ultimate burial depths (Fig. 7a). The cumulative marsh thickness at each location was divided by the entire deltaic deposit thickness to get the marsh fraction in stratigraphy.

This experimental proxy for compressible marsh sediments compacted to less than 25% of its initial thickness under the minor loading (<1kPa) experienced in the experiment. While this mimics some of the subsidence mechanism found in real deltas, the exhaustion of primary consolidation potential within Holocene strata (Keucher, 1994; Keogh, 2020) was not achieved. Additionally, organic-rich field samples experience a high degree of secondary compression due to the collapse of peat particles (Mesri et al., 1997), as well as volumetric losses from oxidation (Chambers et al., 2019). Our marsh proxy is entirely mineral sediment. Even so, the autogenic compaction patterns produced sediment compaction over thicknesses less than a channel depth, providing a compelling comparison to the field.

# 3 Results

## 3.1 Overall Subsidence Trends

Both experiments exhibit measurable subsidence in unchannelized subaerial portions of the delta over timescales of two and ten hours. The quiescent region of measurement varied with delta top channel dynamics, but averaged 0.27 and 0.40 $m^2$ on the ten hour timescale for the control and treatment respectively, resulting in uncertainties less than 25 $\mu$m for each experiment (Fig. 2a, Text S2). Both experiments also exhibit significant spatial and temporal variability. However, the treatment experiment has a significantly higher delta-wide mean subsidence rate of 126 $\mu$m/h compared to 54 $\mu$m/h for the control experiment (over 10 hours; Fig. 2b). Subsidence rates in the treatment experiment usually exceed the threshold for drowning in the absence of river sediment input for stable/unstable marshes (blue dashed line in Fig. 2b corresponding to blue boxes in Fig. 1b), but are lower than the threshold for maximally productive marshes (green dashed line corresponding to green box).

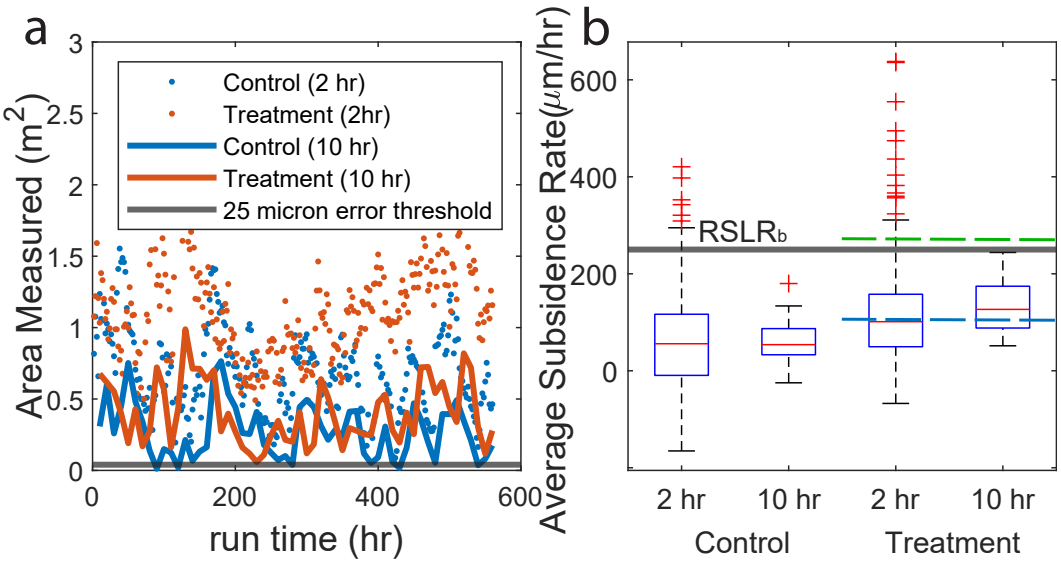


**Figure 2.** (a) Time series of the delta area where Lidar-based subsidence measurements were possible. Note that the number of measurements for the treatment was sufficiently large that error was always less than 25 $\mu$m, and generally less than 10 $\mu$m. (b) Distributions of spatially-averaged subsidence rate for each 2 and 10-hour timestep for both experiments. Boxplots span the $25^{th}$ to $75^{th}$ percentile values, and whiskers extend up to 1.5 times the interquartile range. These subsidence rates are generally greater in the treatment experiment than the control. Dashed green and blue lines represent the thresholds for drowning in maximally productive and stable/unstable marshes respectively.

Subsidence rates (measured over 10 hours) do not show a significant temporal trend over either experiment (Fig. 3c), but regularly fluctuate by more than 100 $\mu$m/h across the delta top. The deposit aggrades from 25 to 165 mm thick at the shoreline throughout the experiment, so the lack of a gradual increase in rates demonstrates that subsidence is uncorrelated with total deposit thickness. Average subsidence rates rarely approach imposed sea level rise ($RSLR_b$=250 $\mu$m/h) for the treatment and never do in the control. Therefore, most of the total relative sea level rise is created by imposed rising base level, as opposed to compactional subsidence, in both cases.

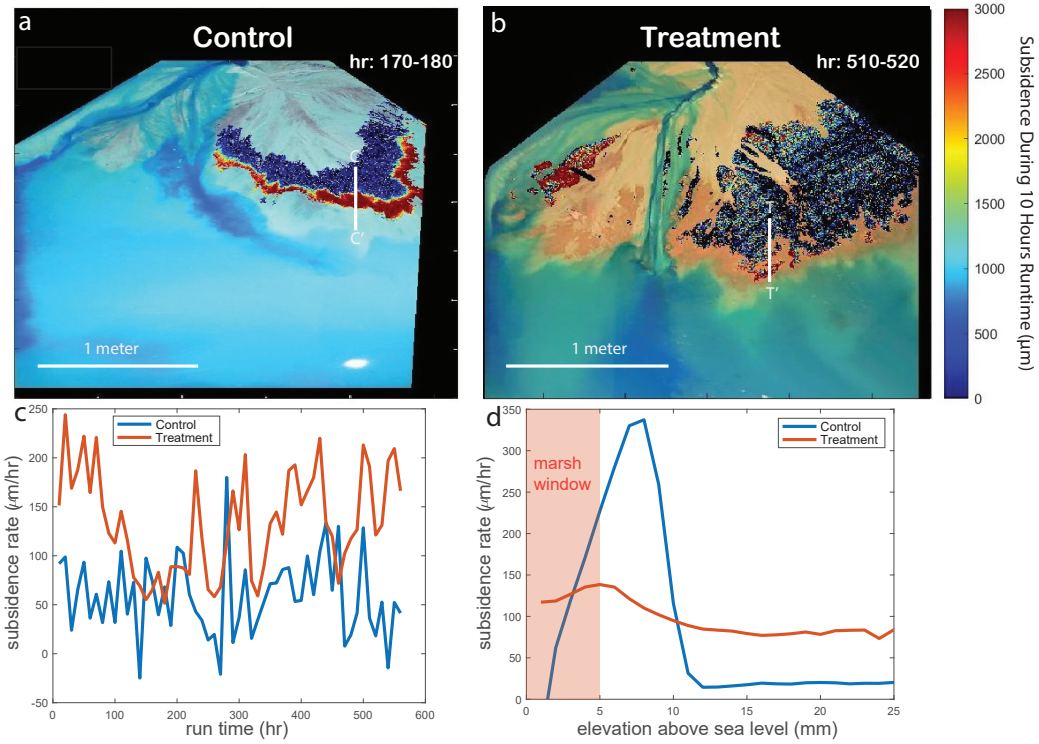


**Figure 3.** (a) Overhead image of control experiment at hour 180 overlain with subsidence map (5 mm x 5 mm resolution) of the previous 10 hours. (b) Overhead image of treatment experiment at hour 520 overlain with subsidence map of the previous 10 hours. (c) Time series of average subsidence rates across the low elevation zone for each ten-hour timestep for both experiments. Subsidence rates are variable through time, but do not exhibit a temporal trend. (d) Time averaged profiles of subsidence as a function of elevation above relative sea level for both experiments. The window of active marsh deposition for the treatment experiment is shaded orange.

Subsidence varies in both experiments as a function of elevation relative to sea level. Subsidence is highly concentrated near the coastline in the control experiment, but more dispersed throughout the subaerial delta and highly spatially variable in the treatment experiment (Fig. 3a, b). Subsidence in the control is clearly related to elevation above sea level (Fig. 3d). Subsidence rates peak at 7-8 mm above sea level and become minimal at around 10 mm above sea level. This subsidence peak moves with the shoreline through transgressions and regressions. It is associated with a slope maximum (Fig. 4a), which consistently occurs 5-10 mm above sea level and backsteps as base level rises. In contrast, the treatment experiment subsidence rates are relatively consistent. Subsidence rates are slightly higher in the window of active marsh deposition, but only decrease by 20-40% in the 20 mm above the marsh window. The subaerial slope break observed in the control (Fig. 4a) is notably absent in the treatment (Fig. 4b), where slopes on the order of several degrees only occur below sea level.

### 3.2 Treatment Experiment Subsidence Pattern and Mechanism

The subsidence patterns in the treatment experiment are more complex than in the control. We study the persistence of subsidence across the delta over a 2-hour timescale. Correlations are drawn by gridding each subsidence map into 50 mm x 50 mm blocks,

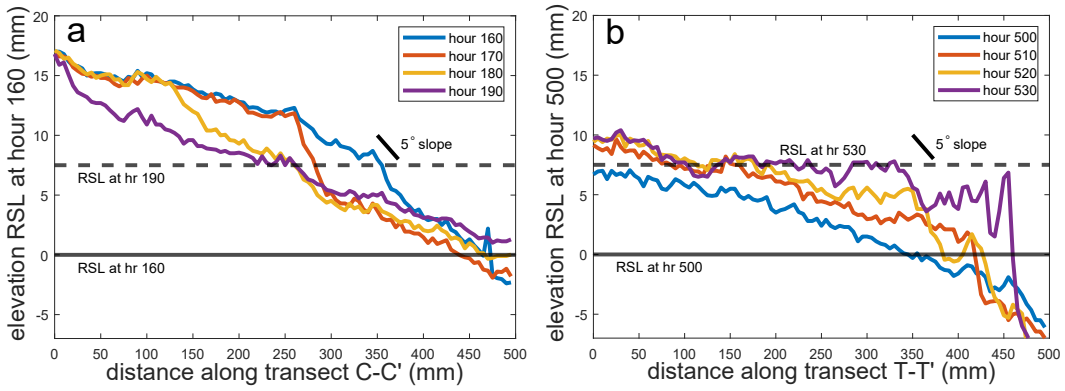


**Figure 4.** (a) Profile of the control experiment topography along transect C-C' from Fig. 3a at hours 160, 170, 180, and 190. Significant bed lowering occurs above sea level and landward of a subaerial slope break. (b) Profile of the treatment topography along transect T-T' from Fig. 3b at hours 500, 510, 520, and 530. No subaerial slope break is present here. The profile is net aggradational everywhere over this time period in spite of subsidence because of marsh deposition (especially from 200-350 mm along transect).

averaging values within every block, and plotting the subsidence rate at each block against either the subsidence rate at each block 2 hours later or the immediately preceding marsh thickness at each block. Subsidence rates are highly transient through time at the 2-hour scale, with subsidence rarely showing significant correlation (R>0.5) over subsequent maps (n=280; orange histogram in Fig. 5). This means that subsidence "hot spots" rarely persist through repeated measurements at the same location.

Local subsidence rates correlate somewhat better with the thickness of the most recent marsh deposit (blue histogram in Fig. 5), with correlations (R) typically ranging from 0.3 to 0.6 for a 2-hour timestep. This marginal correlation declines when comparing 2-hour subsidence to deposition rates averaged over four or six hours. Consequently, very recent marsh deposition rates have some predictive capability over future subsidence rates.

Despite limited short timescale predictability, there is a better correlation between marsh presence and subsidence evaluated over the entire experiment. The fraction of the total stratigraphic package comprised of marsh deposits is measured both directly (Section 2.2), and by summing all individual marsh deposit thicknesses. Though the summed marsh map approach excludes marsh deposited below sea level, and thus underestimates marsh fraction, the two methods follow a similar trend (Fig. 6b). Both methods also correlate well with average subsidence rates throughout the experiment as a function of distance downstream of the entrance channel (Fig. 6c,d). Each measurement type peaks around the average shoreline position, which is located about 1100 mm from the entrance channel (Fig. 6a; K. M. Sanks et al. (2022)). In other words, long-term subsidence rates are higher where marsh deposits are more common.

Stratigraphic measurements of porosity (transformed to void ratio) collected from marsh stratigraphy are used to constrain the vertical profile of subsidence. The void ratio of marsh deposits monotonically decreases with burial depth ($z$; in mm). It is well fit by an exponential decay function $e(z) = 13.21^{-1.54z}$ with an $R^2$ of 0.76. Under conservation of mass and assuming a constant marsh aggradation rate equal to $RSLR_b$, the compaction rate $s$ at any $z$ is $s = RSLR_b * de/dz$, and the total subsidence at any elevation is $s$ integrated from maximum depth (here 170 mm) to depth z:

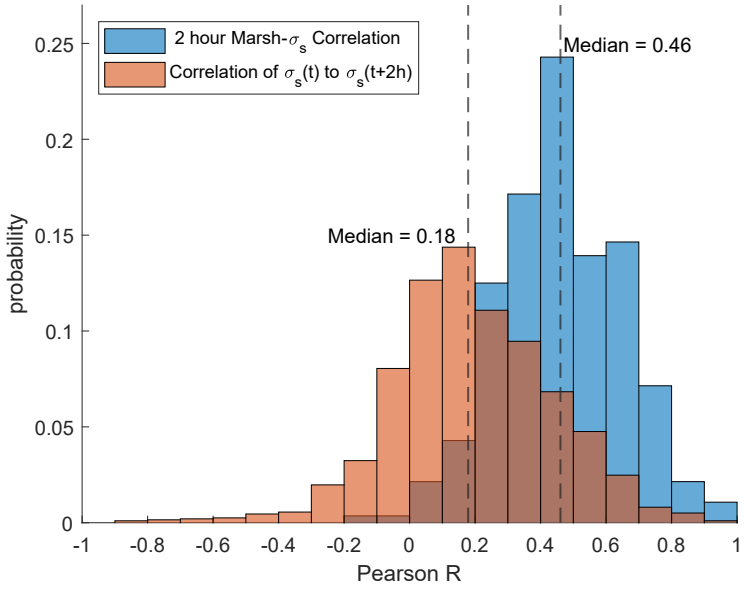


**Figure 5.** Histograms showing the distribution of correlation coefficients (Pearson R) between all local subsidence rates from one timestep to the next (in orange), and between all local subsidence and the most recent marsh deposit thickness (in blue) in the treatment experiment. Median Pearson R values for both histograms are also shown.

$$\sigma_s(z) = \int_{max(z)}^{z} sdz. \tag{1}$$

Subsidence rates calculated in this way assume a steady input of uncompacted marsh (90% porosity) every 2 hours. If the likelihood of marsh deposition is assumed to be unchanging through time, areas that received marsh 50% of the time (with the remainder assumed to be incompressible fluvial sediment) would have 50% of the calculated subsidence rate in this steady-state compaction model.

The majority of the subsidence in the treatment experiment is associated with the compaction of marsh deposits within 20 mm of the surface, and nearly half occurs above one typical channel depth (Fig. 7b). Surface subsidence rates in the compaction model agree well with 10-hour Lidar measurements of surface subsidence clipped to areas actively receiving marsh window. Agreement is particularly good when the subsidence model assumes marsh deposition comprises 25-50% of aggradation with the remainder incompressible fluvial sediments. Much of the delta is comprised of 15-30% marsh deposits (Fig. 6a; K. M. Sanks et al. (2022)). These two independent measurement techniques yield a consistent picture of shallow subsidence in the treatment experiment.

## 4 Discussion

The experimental results presented in this paper suggest that the spatial and temporal structure of shallow subsidence rates are strongly influenced by the presence of compressible marsh deposits in low elevation areas of river deltas. The control experiment exhibited a tight band of subsidence just above sea level. Subsidence patterns in the treatment experiment are widely dispersed and temporally unpredictable at short timescales,

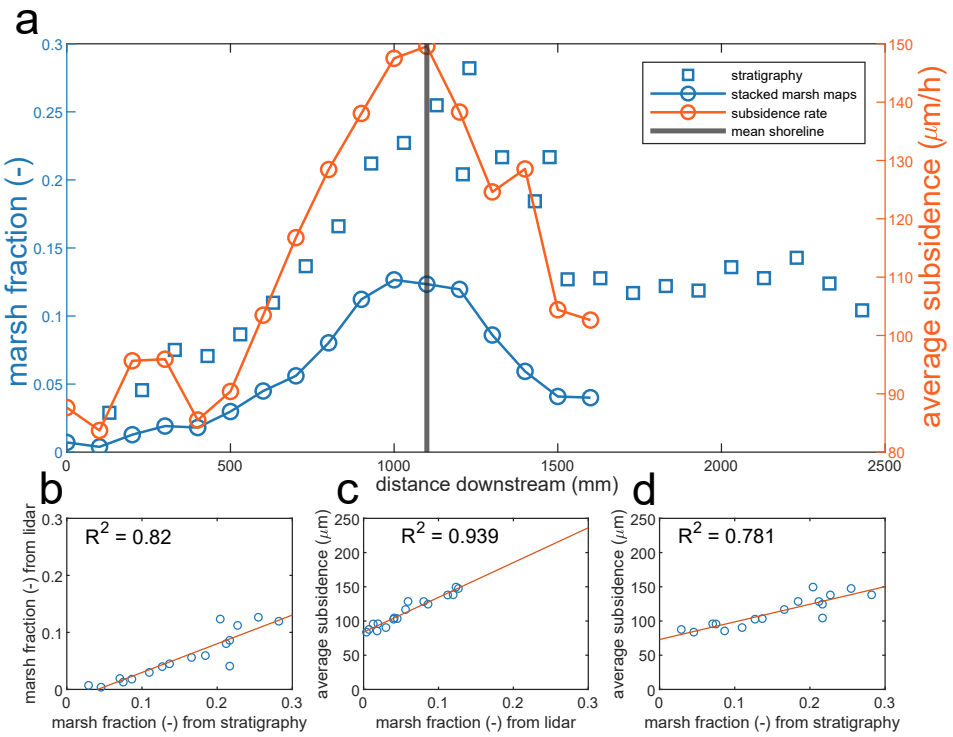


**Figure 6.** Subsidence rate, marsh fraction from stacked marsh maps, and marsh fraction measured from stratigraphy are compared as a function of distance downbasin from the feeder channel. (a) Each parameter peaks around the average shoreline position of 1100 mm downstream of the entrance channel. (b-d) Pair-wise correlation between the three parameters in (a).

but are ultimately predicted by the presence of marsh deposits over long timescales. Scaling subsidence rates by backround relative sea level rise ($\sigma_s/RSLR_b$), we see that the control experiment was 0.2, the treatment experiment was 0.5, and some modern field measurements range between 0.95 and 3.8 (Table 2). While subsidence relative to background relative sea level rise is larger on field scale deltas, the experimental treatment increased compactional subsidence on in the laboratory experiment.

We did not anticipate any subsidence in the control experiment, yet it revealed a well-organized signature. We interpret the subsidence in the control experiment to be compaction from soil creep near sea level. Creep is commonly experienced in coastal areas such as salt marshes and plays a role in bed lowering at a local scale (Mariotti, 2016). Unlike purely vertical sediment consolidation (Terzaghi, 1943), which occurs as pore water is expelled, creep can be triggered by a rising water table decreasing friction between grains and causing failure (Mariotti et al., 2019). The water table rises with $RSLR_b$, so creep is deemed the most likely mechanism triggering the "subsidence" band.

Where can we expect to find this creep style subsidence beyond our control experiment? It is likely to be found in other laboratory delta experiments with rising sea levels, and particularly those using the "strongly cohesive" sediment that includes significant fine grain fractions and a polymer to increase cohesion. While creep has been demon-

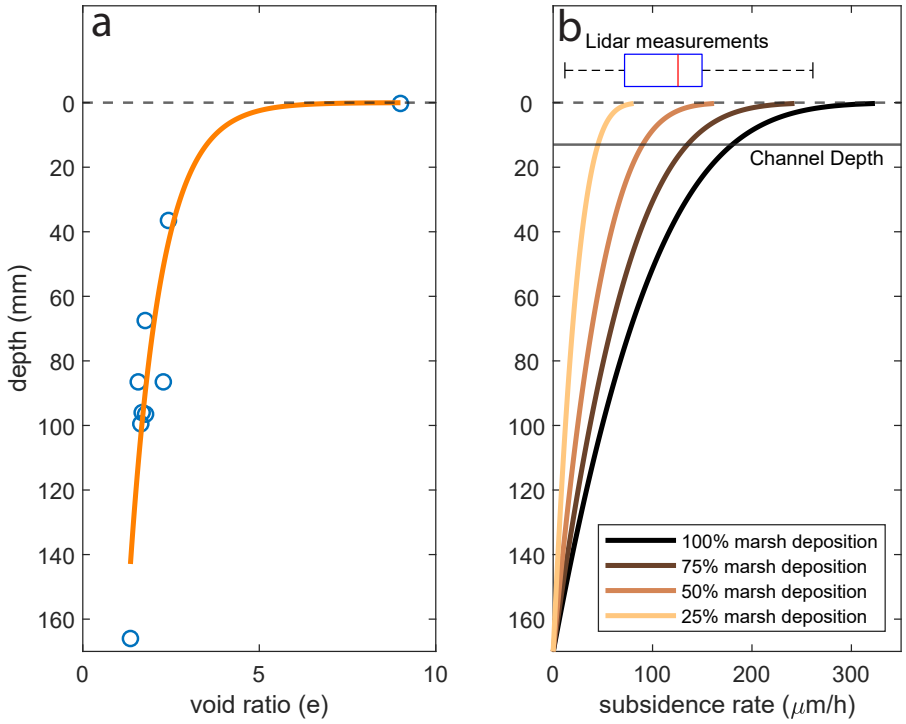


**Figure 7.** Subsidence within marsh deposits calculated from measurements of void ratio within the final deposit. (a) Void ratio as a function of depth. Circles indicate measurements, with exponential fit (see Section 2.2). (b) Subsidence rate with depth for marsh deposits calculated from eq 1. 100% marsh deposition represents a scenario where marsh is always deposited equal to $RSLR_b$ and never eroded. Spatially averaged, 10-hr subsidence rates from Lidar measurements for all areas within the marsh window and average channel depth in the treatment experiment are also shown.

strated in coastal environments, we know of no field data that shows such tight elevation-control of subsidence rates.

By comparison, the treatment experiment produces subsidence that was larger in magnitude and more widespread (Figs. 2, 3). Significant subsidence occurs outside of the marsh window (Fig. 3d). Because the addition of marsh is the only change between experiments, this suggests that marsh sedimentation is influencing subsidence outside the active marsh window. This is unexpected because subsidence is shallow and weakly correlated with recent deposit thickness. This discrepancy can be explained by the fact that a large portion of subsidence in the treatment experiment is controlled by surficial compaction of clay layers, but a degree of marsh deposit compaction continues to occur for some time post-burial (Fig. 7).

Remarkably, the strong elevation-controlled signature of the control experiment is damped in the treatment. This could be because marsh sedimentation decreases the average delta slope by 50% (K. M. Sanks et al., 2022) in the marsh window, potentially reducing creep-based subsidence. Overall, it seems that marsh sedimentation decreases the slope of the delta, removing the near-shore creep failure mechanism, and adding a more spatially variable mechanism of marsh deposit compaction/consolidation.

The behaviors described above establish that the experiments, and particularly the treatment experiment, have strong spatiotemporal variation in compactional subsidence rates. Therefore, the hot spots of above-average subsidence found at one timestep do not predict continued above-average subsidence (Fig. 4). Similar subsidence hot spots have been found on the Mississippi (Jankowski et al., 2017; R. A. Morton et al., 2003; Karengar et al., 2015), Ganges-Brahmaputra (Higgins et al., 2014), and Po (Teatini et al., 2011) deltas. While groundwater pumping and land use can cause persistent subsidence hotspots (Jones et al., 2016), our results show that there may be significant natural temporal variability in compactional subsidence as well.

Recent research comparing bulk densities of Mississippi River Delta sediments over a wide range of lithologies and burial depths shows that most subsidence occurs due to compaction within the upper 10 m of sediment (Jankowski et al., 2017; Keogh, 2020; Zumberge et al., 2022), or even deposits less than 100 years old and well within a meter of the surface (Keogh, 2020). Similarly, compactional subsidence rates in the Ganges-Brahmaputra Delta decay exponentially with depth, with the majority occurring within approximately 1-2 channel depths, or about 25-50 m (Steckler et al., 2022). These findings match well with the exponential decay in subsidence rates with depth found in the treatment experiment (Fig. 7). In both field and experimental settings, most subsidence is occurring in recent marsh deposits shallower than one channel depth. This near surface bed lowering is continuously replenished by new marsh accretion and therefore does not contribute much to the long-term generation of accommodation, as $\sigma_s$ accounts for only about one quarter of $RSLR_b$ below a channel depth (Fig. 7b). Field (van Asselen, 2011) and modeling (Moodie & Passalacqua, 2021; Liang et al., 2016; Xotta et al., 2022; Kim et al., 2010) studies have repeatedly shown the potential influence of subsidence on surface morphology and kinematics. However, they require subsidence to be sufficiently deep-seated for the geomorphic features themselves (channels, levees, etc) to differentially subside. The treatment experiment, along with the preponderance of field data, suggest that compactional subsidence is largely too shallow to impact surface processes.

The treatment experiment represents a first pass at understanding coupling between river deltas and marshes. Future work will link dynamic subsidence rates to marsh platform stability, delta top kinematics, and stratigraphic stacking patterns of coal seams. Continued field and numerical modelling efforts will extend our ability to reliably predict subsidence rates in low elevation coastal zones past the decadal timescale, where they likely remain spatially and temporally variable even under natural conditions.

## 5 Conclusion

This paper represents the first detailed analysis of subsidence within an experimental delta deposit. Subsidence rates in abandoned delta lobes of experiments both treated and untreated with a marsh proxy are non-negligible, at least locally, indicating that they could be an important contributor to total relative sea level rise in cohesive delta experiments. The control experiment experienced rapid bed lowering slightly landward of the coast, likely due to soil creep, but otherwise had subsidence rates near zero. This mechanism may occur in other laboratory experiments that do not include a marsh proxy. In contrast, subsidence patterns in the treatment experiment resemble field scale measurements from the Mississippi River Delta and some global deltas in their spatial and temporal heterogeneity over short timescales, contribution to total relative sea level rise, mechanism of shallow compaction, and correlation with marsh deposition near the shoreline. The compaction of buried marsh deposits which are analogous to peat/coal layers at depth appears to be relatively less important than surficial compaction. These experimental results give valuable predictions of shallow subsidence in space and time that can inform management, modeling, and sustainability initiatives for global deltas.

**Table 2.** Relative importance of compactional subsidence ($\sigma_s$) vs allogenic relative sea level rise ($RSLR_b$) for field scale, experimental, and modelled river deltas at a range of timescales. Rates for Mississippi (Nienhuis et al., 2017), Po (Syvetski et al., 2009; Bruno et al., 2017), and Mekong (Erban et al., 2014; Ishii et al., 2021) are based on modern measurements. Millennial scale rates for the Mississippi (Törnqvist et al., 2008) and longer timescale rates from a hydrodynamic compaction model (Kooi & de Vries, 1998) are included to compare subsidence measurements at different timescales. $RSLR_b$ were estimated for field deltas by adding 1 mm/yr of deep-seated subsidence to eustatic sea level rise rates. The compensation timescale is defined as the mean channel depth divided by the long term aggradation rate (or $RSLR_b$ in the experiments.

| Delta | $\sigma_s$ (mm/y) (µm/h) | RSLRb (mm/y) (µm/h) | $\sigma_s/RSLR_b$ (-) | Timescale of Measurement, tmeas (y), *(h) | Compensation Timescale, tcomp (y), *(h) |
|---|---|---|---|---|---|
| Control (TDB-18) | *54 | *250 | 0.22 | *2-10 | *58.4 |
| Treatment (TDWB-19-2) | *126 | *250 | 0.50 | *2-10 | *53.6 |
| Modern Mississippi | 7.1 | 4.3 | 1.66 | 10 | ~$10^5$ |
| Modern Mekong | 16 | 4.2 | 3.81 | ~10 | ~$3*10^4$ |
| Modern Po | 4 | 4.2 | 0.95 | ~10 | ~$2*10^4$ |
| Holocene Mississippi | 1-5 | ~1.5 | 0.67-3.33 | ~$10^3$ | ~$10^5$ |
| Hydrodynamic Model | 0.1-1 | ~1 | 0.1-1 | ~$5 * 10^4$ | ~$10^5$ |

## 6 Data Availability Statement

The data needed to reproduce the results in this study can be found at: `https://figshare.com/articles/dataset/Subsidence_Experimental_Deltas/21197728`, or (Zapp, 2022b). These data can then be used to reproduce the results of this study when processed with the software located at: `https://github.com/SamZapp/Subsidence_Experimental_Deltas` or (Zapp, 2022a). Raw experimental data is also available for TDB-18-1 (K. Straub & Dutt, 2022), and TDWB-19-2 (K. Sanks et al., 2022).

**Acknowledgments**

The project was funded by an NSF grant (co PIs Kyle Straub; NSF EAR-1848994 that funded Kyle Straub and Jose Silvestre's time plus much of the experimental costs and John Shaw; NSF EAR-1848993 that funded John Shaw and Samuel Zapp's time plus some experimental costs). We have no known conflicts of interest. J. B. Shaw and K. M. Straub funded by the National Science Foundation.

## References

Bruno, L., Amorosi, A., Severi, P., & Costagli, B. (2017, March). Late Quaternary aggradation rates and stratigraphic architecture of the southern Po Plain, Italy. *Basin Research*, *29*(2), 234–248. Retrieved 2022-09-30, from https://www.earthdoc.org/content/journals/10.1111/bre.12174 (Publisher: European Association of Geoscientists & Engineers) doi: 10.1111/bre.12174

Byrnes, M. R., Britch, L. D., Berlinghoff, J. L., Johnson, R., & Khalil, S. (2019). Recent subsidence rates for Barataria Bay, Louisiana. *Geo-Marine Letters*, *39*, 265–278. doi: https://doi.org/10.1007/s00367-019-00573-3

Cahoon, D. R., Lynch, J. C., Roman, C. T., Schmit, J. P., & Skidds, D. E. (2019, January). Evaluating the Relationship Among Wetland Vertical Development, Elevation Capital, Sea-Level Rise, and Tidal Marsh Sustainability. *Estuaries and Coasts*, *42*(1), 1–15. Retrieved 2022-04-07, from https://doi.org/10.1007/s12237-018-0448-x doi: 10.1007/s12237-018-0448-x

Chambers, L. G., Steinmuller, H. E., & Breithaupt, J. L. (2019). Toward a mechanistic understanding of "peat collapse" and its potential contribution to coastal wetland loss. *Ecology*, *100*(7), e02720. Retrieved 2022-09-28, from https://onlinelibrary.wiley.com/doi/abs/10.1002/ecy.2720 (_eprint: https://onlinelibrary.wiley.com/doi/pdf/10.1002/ecy.2720) doi: 10.1002/ecy.2720

Chang, C., Mallman, E., & Zoback, M. (2014, June). Time-dependent subsidence associated with drainageinduced compaction in Gulf of Mexico shales bounding a severely depleted gas reservoir. *AAPG Bulletin*, *98*(6), 1145–1159. doi: 10.1306/11111313009

Couvillion, B. R., Beck, H., Schoolmaster, D., & Fischer, M. (2017). *Land area change in coastal Louisiana (1932 to 2016)* (USGS Numbered Series No. 3381). Reston, VA: U.S. Geological Survey. Retrieved 2018-11-07, from http://pubs.er.usgs.gov/publication/sim3381 (IP-085820)

Dokka, R. K. (2006, April). Modern-day tectonic subsidence in coastal Louisiana. *Geology*, *34*(4), 281–284. doi: 10.1130/G22264.1

Engle, V. D. (2011). Estimating the Provision of Ecosystem Services by Gulf of Maxico Coastal Wetlands. *Wetlands*, *31*, 179–193. doi: https://doi.org/10.1007/s13157-010-0132-9

Erban, L. E., Gorelick, S. M., & Zebker, H. A. (2014). Groundwater extraction, land subsidence, and sea-level rise in the Mekong Delta, Vietnam. *Environmental Research Letters*, *9*. doi: 10.1088/1748-9326/9/8/084010

Frederick, B. C., Blum, M., Fillon, R., & Roberts, H. (2019). Resolving the contributing factors to Mississippi Delta subsidence: Past and Present. *Basin Research*, *31*, 171–190. doi: 10.1111/bre.12314

Higgins, S. A., Overeem, I., Steckler, M. S., Syvitski, J. P. M., Seeber, L., & Akhter, S. H. (2014). InSAR measurements of compaction and subsidence in the Ganges-Brahmaputra Delta, Bangladesh. *Journal of Geophysical Research: Earth Surface*, *119*(8), 1768–1781. Retrieved 2022-09-10, from https://onlinelibrary.wiley.com/doi/abs/10.1002/2014JF003117 (_eprint: https://onlinelibrary.wiley.com/doi/pdf/10.1002/2014JF003117) doi: 10.1002/2014JF003117

Hoyal, D. C. J. D., & Sheets, B. A. (2009). Morphodynamic evolution of experimental cohesive deltas. *Journal of Geophysical Research*, *114*.

Ishii, Y., Tamura, T., & Ben, B. (2021, February). Holocene sedimentary evolution of the Mekong River floodplain, Cambodia. *Quaternary Science Reviews*, *253*, 106767. Retrieved 2022-09-30, from https://linkinghub.elsevier.com/retrieve/pii/S0277379120307290 doi: 10.1016/j.quascirev.2020.106767

Jankowski, K. L., Tornqvist, T. E., & Fernandes, A. M. (2017, March). Vulnerability of Louisiana's coastal wetlands to present-day rates of relative sea-level rise. *Nature Communications*, 1–7. doi: 10.1038/ncomms14792

Jones, C. E., An, K., Blom, R. G., Kent, J. D., Ivins, E. R., & Bekaert, D. (2016). Anthropogenic and geologic influences on subsidence in the vicinity of New Orleans, Louisiana. *Journal of Geophysical Research: Solid Earth*, *121*(5), 3867–3887. Retrieved 2022-09-10, from https://onlinelibrary.wiley.com/doi/abs/10.1002/2015JB012636 (_eprint: https://onlinelibrary.wiley.com/doi/pdf/10.1002/2015JB012636) doi: 10.1002/2015JB012636

Karengar, M. A., Dixon, T. H., & Malservisi, R. (2015). A three-dimensional surface velocity field for the Mississippi Delta: Implications for coastal restoration adn flood potential. *Geology*. doi: 10.1130/G36598.1

Keogh, M. E. (2020). *Accretion, Compaction, and Restoration: Sediment Dynamics and Relative Sea-Level Rise in Coastal Wetlands* (unpublished PhD dissertation). Tulane University, New Orleans, La.

Keucher, G. (1994). *Geologic Framework and Consolidation Settlement Potential of the Lafourche Delta, Topstratum Valley Fill; Implications for Wetland Loss in Terrebonne and Lafourche Parishes, Louisiana* (PhD). Louisiana State.

Kim, W., Sheets, B. A., & Paola, C. (2010, April). Steering of experimental channels by lateral basin tilting. *Basin Research*, *22*(3), 286–301. Retrieved 2022-10-05, from https://www.earthdoc.org/content/journals/10.1111/j.1365-2117.2009.00419.x (Publisher: European Association of Geoscientists & Engineers) doi: 10.1111/j.1365-2117.2009.00419.x

Kooi, H., & de Vries, J. (1998). Land subsidence and hydrodynamic compaction of sedimentary basins. *Hydrology & Earth System Sciences*, *2*, 159–171.

Li, Q., Matthew Benson, W., Harlan, M., Robichaux, P., Sha, X., Xu, K., & Straub, K. M. (2017). Influence of Sediment Cohesion on Deltaic Morphodynamics and Stratigraphy Over Basin-Filling Time Scales. *Journal of Geophysical Research: Earth Surface*, *122*(10), 1808–1826. Retrieved 2022-10-10, from https://onlinelibrary.wiley.com/doi/abs/10.1002/2017JF004216 (_eprint: https://onlinelibrary.wiley.com/doi/pdf/10.1002/2017JF004216) doi: 10.1002/2017JF004216

Liang, M., Kim, W., & Passalacqua, P. (2016). How much subsidence is enough to change the morphology of river deltas? *Geophysical Research Letters*, *43*(19), 10,266–10,276. Retrieved 2022-03-08, from https://onlinelibrary.wiley.com/doi/abs/10.1002/2016GL070519 (_eprint: https://onlinelibrary.wiley.com/doi/pdf/10.1002/2016GL070519) doi: 10.1002/2016GL070519

*Louisiana's Comprehensive Master Plan for a Sustainable Coast* (Tech. Rep.). (2017). Coastal Protection and Restoration Authority. Retrieved 2022-09-28, from https://coastal.la.gov/our-plan/2017-coastal-master-plan/

Mariotti, G. (2016). Revisiting salt marsh resilience to sea level rise: Are ponds responsible for permanent land loss? *Journal of Geophysical Research: Earth Surface*, *121*(7), 1391–1407. Retrieved 2022-03-11, from https://onlinelibrary.wiley.com/doi/abs/10.1002/2016JF003900 (_eprint: https://onlinelibrary.wiley.com/doi/pdf/10.1002/2016JF003900) doi: 10.1002/2016JF003900

Mariotti, G. (2020, October). Beyond marsh drowning: The many faces of marsh loss (and gain). *Advances in Water Resources*, *144*, 103710. Retrieved 2021-04-28, from https://www.sciencedirect.com/science/article/pii/S030917082030395X doi: 10.1016/j.advwatres.2020.103710

Mariotti, G., Kearney, W. S., & Fagherazzi, S. (2019, June). Soil creep in a mesotidal salt marsh channel bank: Fast, seasonal, and water table mediated. *Geomorphology*, *334*, 126–137. Retrieved 2021-06-20, from https://www.sciencedirect.com/science/article/pii/S0169555X1930087X doi: 10.1016/j.geomorph.2019.03.001

Meckel, T., ten Brink, U., & Williams, S. (2006). Current subsidence rates due to compaction of Holocene sediments in southern Louisiana. *Geophysical Research Letters*, *33*. doi: 10.1029/2006GL026300

Mesri, G., Stark, T., Ajlouni, M., & Chen, M. (1997, May). Secondary Compression of Peat With or Without Surcharging. *Journal of Geotechnical and Geoenvironmental Engineering*, *123*(5), 411–421.

Moodie, A. J., & Passalacqua, P. (2021). When Does Faulting-Induced Subsidence Drive Distributary Network Reorganization? *Geophysical Research Letters*, *48*(22), e2021GL095053. (Publisher: Wiley Online Library)

Morris, J. T., Sundareshwar, P., Nietch, C. T., Kjerfve, B., & Cahoon, D. (2002). Responses of Coastal Wetlands to Rising Sea Level. *Ecology*, *83*(10), 2869–2877. doi: https://doi.org/10.1890/0012-9658(2002)083[2869:ROCWTR]2.0.CO;2

Morton, R., Bernier, J., & Barras, J. (2006). Evidence of regional subsidence and associated interior wetland loss induced by hydrocarbon production, Gulf Coast region, USA. *Environmental Geology*, *50*(2), 14. Retrieved 2022-03-08, from http://pubs.er.usgs.gov/publication/70030503 (Code: Environmental Geology Type: Journal Article) doi: 10.1007/s00254-006-0207-3

Morton, R. A., Tiling, G., & Ferina, N. F. (2003, June). Causes of hot-spot wetland loss in the Mississippi delta plain. *Environmental Geosciences*, *10*(2), 71–80. Retrieved 2018-11-07, from https://pubs.geoscienceworld.org/eg/article/10/2/71/61210/causes-of-hot-spot-wetland-loss-in-the-mississippi doi: 10.1306/eg.04040302007

Nienhuis, J. H., Törnqvist, T. E., Jankowski, K. L., Fernandes, A. M., & Keogh, M. E. (2017, September). A New Subsidence Map for Coastal Louisiana. *GSA Today*, 60–61. Retrieved 2018-11-07, from http://www.geosociety.org/gsatoday/groundwork/G337GW/abstract.htm doi: 10.1130/GSATG337GW.1

Paola, C., Straub, K., Mohrig, D., & Reinhardt, L. (2009). The "unreasonable effectiveness" of stratigraphic and geomorphic experiments. *Earth-Science Reviews*, *97*, 1–43. doi: 10.1016/j.earscirev.2009.05.003

Sanks, K., Zapp, S., Silvestre, J., Shaw, J., & Straub, K. (2022, April). TDWB-19-2-Surface-Processes. Retrieved 2022-10-10, from http://sead-published.ncsa.illinois.edu/seadrepository/api/researchobjects/urn:uuid:6242252de4b05d1c54a80ecd (Publisher: SEAD Type: dataset) doi: 10.26009/s0UQYZ0M

Sanks, K. M., Shaw, J. B., & Naithani, K. (2020). Field-Based Estimate of the Sediment Deficit in Coastal Louisiana. *Journal of Geophysical Research: Earth Surface*, *125*(8), e2019JF005389. Retrieved 2022-01-31, from https://onlinelibrary.wiley.com/doi/abs/10.1029/2019JF005389 (_eprint: https://onlinelibrary.wiley.com/doi/pdf/10.1029/2019JF005389) doi: 10.1029/2019JF005389

Sanks, K. M., Zapp, S. M., Silvestre, J. R., Shaw, J. B., Dutt, R., & Straub, K. M. (2022). Marsh Sedimentation Controls Delta Top Morphology, Slope, and Mass Balance. *Geophysical Research Letters*, *49*(12), e2022GL098513. Retrieved 2022-09-07, from https://

onlinelibrary.wiley.com/doi/abs/10.1029/2022GL098513 (_eprint: https://onlinelibrary.wiley.com/doi/pdf/10.1029/2022GL098513) doi: 10.1029/2022GL098513

Shirzaei, M., Freymueller, J., Törnqvist, T. E., Galloway, D. L., Dura, T., & Minderhoud, P. S. J. (2021, January). Measuring, modelling and projecting coastal land subsidence. *Nature Reviews Earth & Environment*, *2*(1), 40–58. Retrieved 2022-10-10, from https://www.nature.com/articles/s43017-020-00115-x (Number: 1 Publisher: Nature Publishing Group) doi: 10.1038/s43017-020-00115-x

Steckler, M. S., Oryan, B., Wilson, C. A., Grall, C., Nooner, S. L., Mondal, D. R., ... Goodbred, S. L. (2022, January). Synthesis of the distribution of subsidence of the lower Ganges-Brahmaputra Delta, Bangladesh. *Earth-Science Reviews*, *224*, 103887. Retrieved 2021-12-22, from https://www.sciencedirect.com/science/article/pii/S0012825221003883 doi: 10.1016/j.earscirev.2021.103887

Straub, K., & Dutt, R. (2022, March). TDB-18. Retrieved 2022-10-10, from http://sead-published.ncsa.illinois.edu/seadrepository/api/researchobjects/urn:uuid:62408a5ce4b05d1c54a80412 (Publisher: SEAD Type: dataset) doi: 10.26009/s0G2SM3L

Straub, K. M., Li, Q., & Benson, W. M. (2015). Influence of sediment cohesion on deltaic shoreline dynamics and bulk sediment retention: A laboratory study. *Geophysical Research Letters*, *42*(22), 9808–9815. Retrieved 2022-10-10, from https://onlinelibrary.wiley.com/doi/abs/10.1002/2015GL066131 (_eprint: https://onlinelibrary.wiley.com/doi/pdf/10.1002/2015GL066131) doi: 10.1002/2015GL066131

Syvetski, J., Kettner, A., Overeem, I., Hutton, E., Hannon, M., Brackenridge, G. R., ... Nichols, R. (2009). Sinking deltas due to human activities. *Nature Geoscience*, *2*, 681–686. doi: https://doi.org/10.1038/ngeo629

Teatini, P., Tosi, L., & Strozzi, T. (2011). Quantitative evidence that compaction of Holocene sediments drives the present land subsidence of the Po Delta, Italy. *Journal of Geophysical Research: Solid Earth*, *116*(B8). Retrieved 2022-09-30, from https://onlinelibrary.wiley.com/doi/abs/10.1029/2010JB008122 (_eprint: https://onlinelibrary.wiley.com/doi/pdf/10.1029/2010JB008122) doi: 10.1029/2010JB008122

Terzaghi, K. (1943). *Theoretical Soil Mechanics*. New York: Wiley.

Tornqvist, T. E., Jankowski, K. L., Yong-Xiang, L., & Gonzalez, J. L. (2020, May). Tipping points of Mississippi Delta Marshes due to accelerated sea-level rise. *Science Advances*, *6*(21). doi: 10.1126/sciadv.aaz5512

Törnqvist, T. E., Wallace, D. J., Storms, J. E. A., Wallinga, J., van Dam, R. L., Blaauw, M., ... Snijders, E. M. A. (2008, March). Mississippi Delta subsidence primarily caused by compaction of Holocene strata. *Nature Geoscience*, *1*(3), 173–176. Retrieved 2018-11-07, from https://www.nature.com/articles/ngeo129 doi: 10.1038/ngeo129

van Asselen, S. (2011). The contribution of peat compaction to total basin subsidence: implications for the provision of accomodation space in organic-rich deltas. *Basin Research*, *23*, 239–255. doi: 10.1111/j.1365-2117.2010.00482.x

Xotta, R., Zoccarato, C., Minderhoud, P. S. J., & Teatini, P. (2022). Modeling the Role of Compaction in the Three-Dimensional Evolution of Depositional Environments. *Journal of Geophysical Research: Earth Surface*, *127*(9), e2022JF006590. Retrieved 2022-09-10, from https://onlinelibrary.wiley.com/doi/abs/10.1029/2022JF006590 (_eprint: https://onlinelibrary.wiley.com/doi/pdf/10.1029/2022JF006590) doi: 10.1029/2022JF006590

Yuill, B., Lavoie, D., & Reed, D. (2009). Understanding subsidence processes in coastal Louisiana. *Journal of Coastal Research*(54), 23–36.

Zapp, S. (2022a, October). SamZapp/Subsidence_experimental_deltas:v1. *Zenodo*. doi: 10.5281/zenodo.7183295

Zapp, S. (2022b, October). Subsidence_experimental_deltas. Retrieved 2022-10-10, from `https://figshare.com/articles/dataset/Subsidence_Experimental_Deltas/21197728/1` (Publisher: figshare Type: dataset) doi: 10.6084/m9.figshare.21197728.v1

Zumberge, M. A., Xie, S., Wyatt, F. K., Steckler, M. S., Li, G., Hatfield, W., ... Törnqvist, T. E. (2022). Novel Integration of Geodetic and Geologic Methods for High-Resolution Monitoring of Subsidence in the Mississippi Delta. *Journal of Geophysical Research: Earth Surface*, *127*(9), e2022JF006718. Retrieved 2022-09-10, from `https://onlinelibrary.wiley.com/doi/abs/10.1029/2022JF006718` (_eprint: https://onlinelibrary.wiley.com/doi/pdf/10.1029/2022JF006718) doi: 10.1029/2022JF006718